COMPUTATION OF TWO DIMENSIONAL VORTEX SHEET ROLL UP

John Steinhoff
The University of Tennessee Space Institute
Tullahoma, TN 37388

Abstract

We describe two methods to treat vortex sheets in a Lagrangian manner as a discontinuity, but to compute the rest of the flow using a fixed Eulerian grid. This way, we retain advantages of both schemes. The method is applied to the vortex sheet shed by an elliptically loaded wing, in the parabolized approximation. In this approximation, the vorticity is assumed to be normal to a two dimensional cross-stream computational plane. Thus the sheet is treated as a line across which the cross-stream velocity is discontinuous. The stream-wise variation of velocity is then neglected and time evolution of the line in the plane approximates the cross-stream variation as the sheet is followed downstream.

The time-dependent problem is solved as follows: At each time step, the vortex line is first assumed to be fixed and a potential is computed on a grid such that the discontinuity across the line is maintained and Laplace's equation is satisfied everywhere else. Then, a velocity is computed along the line by interpolation from the grid. Finally, a forward Euler integration scheme is used to compute the new position of the line. The main approximation assumed is that the radius of curvatuare of the line is much larger than the grid cell width.

One method described is analagous to shock fitting and involves fitting the discontinuity. The other, presented previously, involves spreading the discontinuity over several grid cells, and is analagous to shock capturing. A numerical comparison of the two schemes is given.

1. Introduction

Computational methods, based on the compressible potential flow or Euler equations, are currently being used to compute three dimensional flows over wings and wing/body combinations [1]. They can adequately account for shocks in the flow and, when coupled with existing boundary layer calculating methods, can include boundary layer effects [2], at least when there are no regions with extensive separation.

Besides boundary layers, which exist in relatively thin regions on surfaces, other important effects result from vortex sheets in the flow. These are also usually confined to thin regions. Unlike boundary layers, their position is not known in advance, but must be computed along with the flow field. These sheets are shed from lifting surfaces and, when convected past other lifting surfaces, can have large effects on the flow. Examples include wing/canard configurations and helicopter rotors. Also, leading edge separation in delta wings or at strakes, can result in vortex sheets moving past the same lifting surface that produced the sheet, also with important effects.

This is especially true in transonic flow with shock waves, where the vortex sheet can cause large movements of the shock and large changes in lift and drag. In addition, even for an isolated wing; proper treatment of the sheet is necessary to avoid large errors in the computed surface pressures near the wing tip.

Numerical methods for solving transonic flow problems, in the inviscid region exterior to boundary layers, usually involve either the Potential Flow or Euler equations. As usually formulated, the Potential Flow equations can only treat vorticity if concentrated in a sheet which coincides with a computational boundary. This precludes, for example, following the rollup of a trailing edge sheet. The Euler equations, on the other hand, can treat flow with vorticity, but concentrated vortex lines to sheets can spread when convected due to numerical diffusion, even when moderate amounts of grid compression are used[3]. Besides this problem, which involves a grid that must adapt to the flow, Euler equations are expensive to solve, requiring much more computing time than Potential Flow equations for the same problem.

In this paper we describe and compare two methods for incorporating vortex sheets into the Potential Flow equations. They are conceptually and practically different than methods used to incorporate vortices into incompressible flow problems [4], and may have advantages there too. The basic iteration sequence, however, is similar. The vortex sheet is assumed to convect with the flow. At each step, first, the sheet is taken to be fixed and the flow field is computed such that the boundary conditions and flow equations are satisfied. Then, the sheet is adjusted to follow the new flow field. This iteration is usually required even in the incompressible case, where the equations are linear and the solution due to the vortex sheet can be added to a solution due to the vortex sheet can be added to a solution without the sheet.

The two methods both involve treating the sheet as a velocity discontinuity. Although designed for

compressible three dimensional problems, both methods are treated in a quasi-two dimensional incompressible approximation. In this approximation, the vortex sheet is assumed to roll up slowly as it convects downstream in incompressible flow. The convection speed is assumed to be the free-stream velocity and the vorticity aligned with the free stream. In this case planes at different downstream positions can be treated as different time steps in a two-dimensional time dependent evolution of a line of vorticity where the vorticity is normal to the plane. This has been a standard testing-ground for methods capable of treating three dimensional incompressible flow [5].

Both of our methods involve treating the sheet as a velocity discontinuity. Also, in both, the velocity outside the sheet is assumed to be irrotational and derived from a potential, which is solved for on a fixed (Eulerian) grid. The first method is, to the author's knowledge, new. It involves following the discontinuity and using a local solution in the region near the sheet, while solving for a potential on a fixed grid. The second method involves spreading the vortex sheet over several grid cells using a velocity decomposition method. It has previously been described [6].

2. Problem Definition

The basic problem consists of solving Laplace's equation for a potential, ϕ. The outer boundary is a rectangle;

$$0 \le x \le +\frac{1}{2}\ ,\ -\frac{1}{2} \le y \le +\frac{1}{2}.$$

Reflection symmetry is imposed at the $x = 0$ boundary and Neumann conditions are used. Dirichlet conditions are imposed on the other three boundaries. These boundaries are too close to be considered far-field for an accurate solution but their influence should not effect the stability and local behavior of the solution, which is what is being studied. Embedded in the field is a line $x_v(s), y_v(s)$, across which ϕ has a given discontinuity $\Gamma(s)$. The other condition imposed on the line is that the normal derivative of ϕ, $\partial_n\phi$, is continuous. This problem is solved at each of a sequence of time steps, and the normal velocity ($q_n^v(s)$) and average of the tangential velocities on each side ($q_s^v(s)$) are computed. A new position of the line is then computed using forward Euler integration:

$$x_v'(s) = x_v(s) + \Delta t \times u_v(s)$$
$$y_v'(s) = y_v(s) + \Delta t \times v_v(s)$$

where Δt is the time step and $u_v(s)$ and $v_v(s)$ are the Cartesian components of $q_n^v(s)$ and $q_s^v(s)$.

3. Methods of Solution

3.1 Discrete Method

To compute ϕ a cartesion grid is set up in the rectangle. The actual potential is smooth except at the discontinuity. If this is properly treated, as long as the curvature of the line and the scale over which $\Gamma(s)$ varies is much greater than the grid spacing, the velocities should be smooth and grid resolution should be adequate. Accordingly, ϕ is treated as a smooth function on either side of the line and continued through to the other side. The continuation involves adding a local analytic solution to ϕ which satisfies the boundary conditions on the line. On one side, the solution is

$$\phi = \phi^+(x,y)$$

and the continuation of ϕ^+ is

$$\phi^+ = \phi^- - \phi^L(s,x,y).$$

The local solution has the correct discontinuity $\Gamma(s)$ and zero normal derivative at the line.

The problem, then, involves solving Laplace's equation for ϕ using the local solution to join the solution on either side. We use a five-point second-order accurate difference scheme

$$\frac{\left(\tilde{\phi}_{i+1,j} - 2\tilde{\phi}_{i,j} + \tilde{\phi}_{i-1,j}\right)}{\Delta x} +$$
$$\frac{\left(\tilde{\phi}_{i,j+1} - 2\tilde{\phi}_{i,j} + \tilde{\phi}_{i,j-1}\right)}{\Delta y} = 0 \qquad (1)$$

for the potential with the discontinuity removed. If the differences in (1) all lie on one side of the line, then we just have the potentials

$$\tilde{\phi}_{k,l} = \phi_{k,l}$$

for each k, l in the formula. If a difference is required across the line, the continuation of ϕ is used for that point on the other side from the central point in the formula (i,j):

$$\tilde{\phi}_{k,l} = \phi_{k,l} \pm \phi^L_{k,l},$$

where $\phi^L_{k,l}$ is the value of $\phi^L(s,x,y)$ at (k,l) and the choice of sign depends on the direction in which the line is crossed (see Fig. 1). With this scheme, we can incorporate $\phi^L_{k,l}$ into a forcing function and derive a Poisson equation for the values of ϕ at all the grid points;

$$\nabla_c^2\phi_{i,j} = \rho_{i,j} \qquad (2)$$

where ∇_c^2 is the five point Laplacian, $\phi_{i,j}$ is just the potential at grid point (i,j) and $\rho_{i,j}$ is either 0 or

$\mp\phi^L_{i',j'}$ where (i',j') denotes the image point corresponding to point i,j on the other side of the line. An ADI solver is used to solve Poisson's equation.

The calculation of ϕ^L proceeds as follows: The line is defined by a set of markers to each of which a given value of discontinuity is assigned (Γ_l). The grid cells that these markers lie in are computed sequentially for each marker (adjacent markers lie in different cells), $(l = 1, 2, \cdots l_v)$ and, when the cell changes the indices of the corners of the cell side that has been traversed are stored. The local solution, ϕ^L, must be computed at these two points $(i,j\ ;\ i',j')$. For a line section with constant curvature and linearly varying potential, ϕ^L on either side can be taken to be the potential of a point vortex located at the center of curvature with strength proportional to $\Gamma(s)$. This would involve extrapolating Γ with constant value along rays normal to the line, since for a point vortex the potential is constant along radial lines. An averaging is introduced at this point which should not effect the result if the actual radius of curvature and the discontinuity vary slowly compared to the grid spacing. The final formula used for ϕ^L is:

$$\phi^L_{i,j} =< \Gamma > = \left(\sum_l f(\mid \vec{r}_{i,j} - \vec{r}_l \mid)\Gamma_l\right)/F$$

$$F = \sum_l f\left(\mid \vec{r}_{i,j} - \vec{r}_l \mid\right)$$

In this equation, $\mid \vec{r}_{i,j} - \vec{r}_l \mid$ is the distance between grid point i,j and line marker l, and the sum is over all l values such that the weighting function

$$f(Z) = 1 - Z^2/a^2$$

is positive. Typically, a is chosen such that the averaging distance, $< Z >= 3a/8$ is about 1.5 grid spacings:

$$a = 2(\Delta x + \Delta y)$$

Once the set $\{\phi^L_{i,j}\}$ is computed and (2) is solved for $\{\phi_{i,j}\}$, the velocities along the line can be solved for. First, a set of velocities are computed at midoints of the grid lines. These velocities are the averages of the "actual" velocity and the velocity of the solution that is continued from the other side of the line. These velocities are needed on the four corners of a box surrounding each marker point, so that an area-weighting interpolation scheme can be used to compute the velocity at the marker:

$$u_l = \Big(A_{22}u_{i,j} + A_{12}u_{i+1,j} + A_{21}u_{i,j+1} + A_{11}u_{i+1,j+1}\Big)/A$$

$$A_{11} = \Big(x_l - x_{ij}\Big)\Big(y_l - y_{ij}\Big)$$

$$A_{12} = \Big(x_l - x_{i,j}\Big)\Big(y_{i,j+1} - y_l\Big)$$

$$A_{21} = \Big(x_{i+1,j} - x_l\Big)\Big(y_l - y_{ij}\Big)$$

$$A_{22} = \Big(x_{i+1,j+1} - x_l\Big)\Big(y_{i+1,j+1} - y_l\Big)$$

$$A = A_{11} + A_{12} + A_{21} + A_{22}$$

and similarly for v_l. Computation of these corner velocities can be done if the values of ϕ_{ij} and ϕ^L_{ij} are known in the cells surrounding that in which the marker lies (see Fig. 2). This velocity calculation requires that the local solution, ϕ^L, be computed at more points than is required for calculation of the potential.

Results are presented in Fig. 3 for a discontinuity that was elliptic at $t = 0$.

$$\Gamma\Big(0,s\Big) = \Gamma_0\sqrt{1 - (s/s_f)^2}$$

$$0 \le x(0) < +s_f$$

$$y(0) = -.02$$

There were 500 markers used initially and a 64 x 128 cell grid. If distance between markers increased to greater than half of a cell width, new markers were added. The non-dimensional time step, $\Delta t \times \Gamma_0$ was .05. In the figure, the (downward) velocity of the initial first marker was subtracted from the rest to keep the line in the computational grid. It can be seen that an instability appears after about $t \approx .75$. Initial experiments where the line is still treated as a zero-width discontinuity but with marker redistribution and time step changes have not altered the basic features of the instability of this particular method.

The velocity interpolation method used above required that ϕ^L be computed at grid points up to two mesh cells from the vortex line. A more compact scheme requiring only those points one mesh cell from the line, which are also needed to compute the right hand side of Poisson's equation (2) was also implemented. Here, the potentials, ϕ^+ and ϕ^-, were computed by interpolation at each point where the vortex line crossed a grid line. These potentials were

then used to compute tangential derivatives of ϕ^+ and ϕ^-. Also at these points one-sided interpolations were used to compute the derivatives of ϕ^+ and ϕ^- along the grid line that was crossed. These derivatives were averaged to get average velocities along the vortex line and along the grid line crossed. Using these two averages, the average velocity normal to the grid line crossed was then computed. This was done at each point that the line crossed a grid line, and the resulting velocities were interpolated to each marker along the line. Results of this scheme are presented in Fig. 4. As to be expected in a more compact scheme, there appears to be less numerical error here and the vortex rollup is considerably tighter. It can also be seen that the same type of instability appears here that appeared when the other interpolation scheme was used.

3.2 Continuum Method

This method was initially described in Ref. (6). It involves treating the line as if it were spread over a distance, δ, equal to several cell widths. The potential, ϕ, is still defined on a grid, but is now assumed to be continuous. A vortical velocity field $\vec{q}^v$ concentrated within a distance δ of the line is added to $\vec{\nabla}\phi$;

$$\vec{q} = \vec{\nabla}\phi + \vec{q}^v \tag{3}$$

Then the incompressibility requirement is enforced by solving Poisson's equation for ϕ:

$$\vec{\nabla} \cdot \vec{q} = 0$$

or

$$\nabla^2\phi = -\vec{\nabla} \cdot \vec{q}^v. \tag{4}$$

The only requirement on $\vec{q}^v$ is that it have the correct vorticity to represent the (spread) discontinuity. If $\vec{q}^v$ is concentrated near the line, it can be shown that it must have a component normal to the line if it is to represent a non-zero total vorticity (see Ref. 6). We took $\vec{q}^v$ to be normal to the line. Then denoting s the tangential direction and n the normal one, the vorticity,

$$\begin{aligned}\omega &= \partial_s q_n - \partial_n q_s \\ &= \partial_s q_n^v\end{aligned}$$

since $\vec{\nabla}\phi$ does not contribute. In order to represent the desired discontinuity, we must have

$$\Gamma(s) = \int dn \cdot \vec{q}^v(n,s) = \int dn q_n^v(n,s)$$

at each point along the line, where the integral crosses the line center at point s. As in (3.1), we represented the line by a set of markers. Then,

$$\vec{q}^v(\vec{v}) = C \sum_l \sigma(\mid \vec{v} - \vec{v}_l \mid)\vec{q}_l^v. \tag{5}$$

where the sum is over markers such that the weighting function, σ, is non-zero, and $\vec{q}_l^v$ is normal to the line at marker l, with magnitude proportional to $\Gamma(s) \times \Delta s$ at that point. (Δs is the marker spacing). The weighting function, $\sigma(Z)$, had a Gaussian form for small Z and was zero for Z greater than several cell widths.

The solution procedure for this method was similar to the last. At each time step $\vec{q}^v$ was computed at grid points near the line center using (5). Then, $\vec{\nabla} \cdot \vec{q}^v$ was computed and (4) was solved for ϕ on the grid. After that, (3) was used to compute $\vec{q}$ at the grid points. The velocity was then interpolated at the marker positions and they were updated using forward Euler integration.

Results are presented in Fig. (5) for this method (see Ref. 6). Initial results for this method in transonic potential flow are presented in Ref (7). This was a test of the feasibility of adding a vortical velocity to a compressible potential flow. There, the compressible full potential equation was solved for steady three dimensional flow. A line vortex convecting past the wing was embedded in the flow and an added vortical velocity used to represent its effect (see Fig. 6). The C_p distributions over different span stations of the wing are presented in Fig. 7 with and without the convecting vortex line. It can be seen that the vortexz has a large effect. Subsequently, other uses of the method for compressible transonic flow have been presented (8). A full three dimensional transonic code including wake rollup using this method is presently being developed.

4. Discussion

Two methods have been presented to compute the time-dependent roll-up of a vortex sheet in two dimensions. At each of a sequence of time steps, both involve the solution of Laplaces' equation for a potential on a grid in a rectangle with Dirichlet conditions on three sides and Neumann on the fourth, and with a given discontinuity along a curve. This solution is used to compute an average velocity along the curve and to derive a new position of the curve at the next time step using forward Euler integration.

The main difference concerns the way the discontinuity is treated: In the first method a local potential solution is used to link the potentials on either side of the discontinuity. This local potential defines a velocity that is irrotational, has the required discontinuity at the line and has zero normal derivative there. This method is analogous to shock fitting procedures. Considerable logic was required to treat the discontinuity with this method.

In the second method, the discontinuity is spread over several mesh cells so that there is a finite-width region with non-zero vorticity. It is argued that as long as the spreading is over a region that is small compared to the other dimensions in the problem, the large scale features of the solution should not be altered. This is analogous to shock-capturing, as pointed out in Ref. (6). The logic required to implement this method was much simpler than that for the previous one.

Both methods are similar to that of Ref. (9) and use a similar Poisson equation, velocity, interpolation and time integration. In Ref. (9) the line is treated as a set of vortices. Each vortex has associated with it a discontinuity which runs along a grid line and connects it to its image. This results in a large number of discontinuities, rather than just the original one. Like our method, that of Ref. (9) can be extended to treat compressible potential flow with embedded vortices.

Conclusion

It appears that our treatment of the vortex sheet as an exact discontinuity leads to grid-dependent irregularities and, eventually instability. Our alternative method, which involves spreading the discontinuity, or vorticity, resulted in a smooth roll-up. The similar method of Ref. (9), which also involved some averaging, also resulted in a fairly smooth roll-up. In Ref. (10), the line was treated as an exact discontinuity. There, a Green's function approach was used, rather than a grid and finite difference scheme. Also, the curve was defined using higher order spline functions. This approach resulted in smooth roll-up. Hence, it appears that an interaction of our grid with the line or our lower order treatment of the line is the cause of the problem with the first method presented. Since the use of the grid for solving for the potential can have large computational advantages over a Green's function method, work should be continued to resolve this problem.

References

1. Baker, T. J. and Forsey, C. R., "A Fast Algorithm for the Calculation of Transonic Flow Over Wing/Body Combinations," AIAA 5th Computational Fluid Dynamics Conference, Palo Alto,CA, pp. 189–198, June 1981.

   Caughey, D. A., "Multi-grid Calculations of Three-Dimensional Transonic Potential Flows," AIAA paper 83-0374, presented at AIAA 21st Aerospace Sciences Meeting, Reno, NV, Jan. 1983.

   Shmilovich, A., and Caughey, D. A., "Application of the Multi-Grid Method to Calculations of Transonic Potential Flow About Wing-Fuselage Combinations," NASA Conference Publication 2202, Oct. 1981.

   Jameson, A., Schmidt, W., and Turkel, E., "Numerical Solutions of the Euler Equations by Finite Volume Methods Using Runge-Kutta Time-Stepping Schemes," AIAA Paper 83-1259, 1981.

   Jameson, A. and Baker, T. J., "Solution of the Euler Equations for Complex Configurations," AIAA Paper No. 83-1929, presented at AIAA Computational Fluid Dynamics Conference, Danvers, MA, July 1983.

2. Streett, C. L., "Viscous-Inviscid Interaction for Transonic Wing-Body Configurations Including Wake Effects," AIAA Journal, Vol. 20, No. 7, pp. 915–923, July, 1982.

   Wigton, L. B., and Yoshihara, H., "Viscous-Inviscid Interactions with a Three-Dimensional Inverse Boundary Layer Code," Second Symposium on Numerical and Physical Aspects of Aerodynamic Flows, California State University, Long Beach, CA, 17-20 January 1983.

   Samant, SS. and Wigton, L. B., "Coupled Euler/Integral Boundary Layer Analysis in Transonic Flow," AIAA Paper No. 83-1806, presented at AIAA Applied Aerodynamics Conference, Danvers, MA, July 1983.

3. G. R. Srinivasan, W. J. Chyu and J. L. Steger, "Computation of Simple Three-Dimensional Wing-Vortex Interaction in Transonic Flow," AIAA Paper 81-1206, June 1981.

4. A. Leonard, "Vortex Methods for Flow Simulation," J. Comp. Phys., Vol. 37, 1980, pp. 289–335.

5. Baker, "The 'Cloud in Cell' Technique Applied to the Rollup of Vortex Sheets," J. Comp. Phys. Vol. 31, 1979, pp. 76–95.

6. J. Steinhoff and K. Suryanarayanan, The Treatment of Vortex Sheets in Compressible Potential Flow, pg. 1, Proceedings, AIAA 6th Computational Fluid Dynamics Conference, Danvers Mass., July, 1980.

7. J. Steinhoff, K. Suryanarayanan and K. Ramchandran, "The Treatment of Convected Vortices in Compressible Potential Flow," AGARD Symposium on Aerodynamics of Vortical Type Flows in Three Dimesnions, (AGARD-CPP-342) Rotterdam, Netherlands, April, 1983.

8. McCroskey, W. J. and Goorjian, P. M., "Interactions of Airfoils with Gusts and Concentrated Vortices in Unsteady Transonic Flow," AIAA Paper 83-1691, AIAA 16th Fluid and Plasma Dynamics Conference, July 1983, Danvers, Mass.

9. E. Murman and P. M. Stremel, "A Vortex Wake Capturing Method for Potential Flow Calculations," AIAA Paper 82-0947, June, 1982.

10. Hoeijmakers, H.W.M. and Vaatstra, W.: A Higher-Order Panel Method Applied to Vortex Sheet Roll-Up, AIAA Journal 21, No. 4 (1983). pp. 516–523.

Acknowledgement

Some of this work was done while the author was at the Lehrstuhl für Luft und Raumfahrt, Technische Hochschule, Aachen. Also, Mr. K. Ramachandran of The University of Tennessee Space Institute has generated the computer plots and provided considerable assistance in running the code.

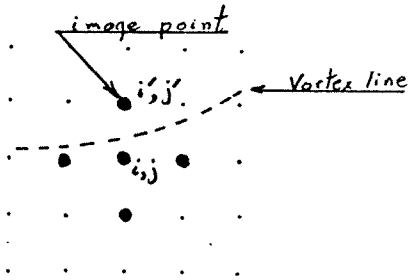

Figure 1. Finite Difference Molecule and Image Point

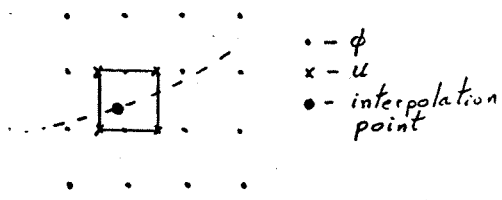

Figure 2. U-Velocity Interpolation

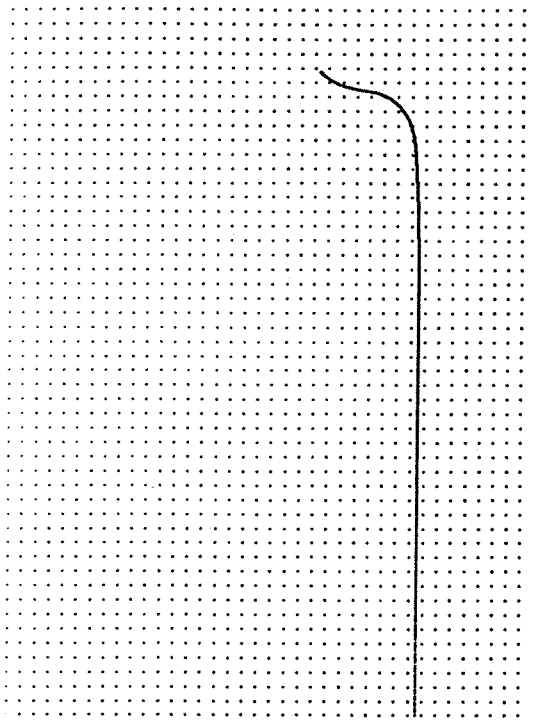

Figure 3a. t=.2

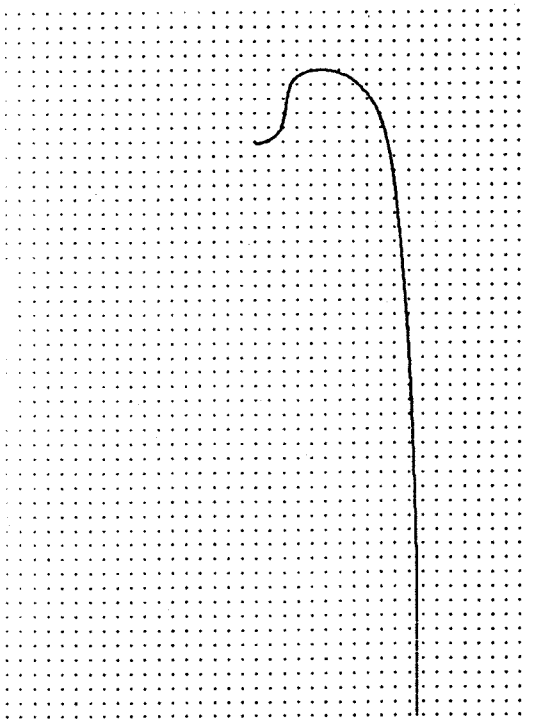

Figure 3b. t=.4

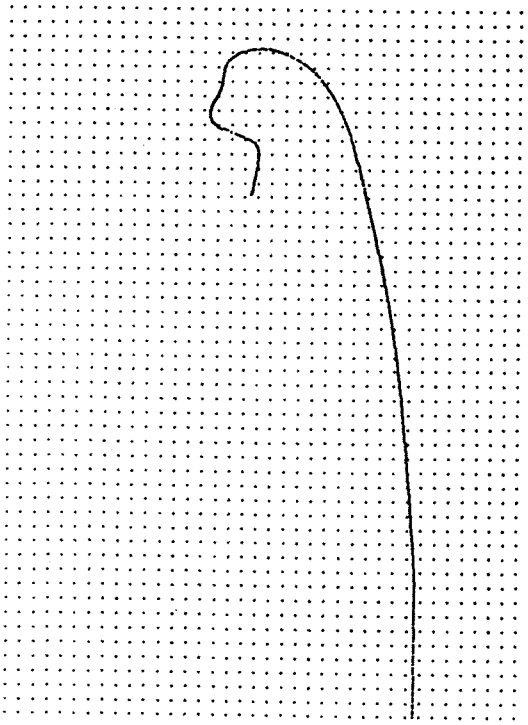

Figure 3c. t=.6

Figure 4a. $.15 \leq t \leq .25$

Figure 4b. $.40 \leq t \leq .50$

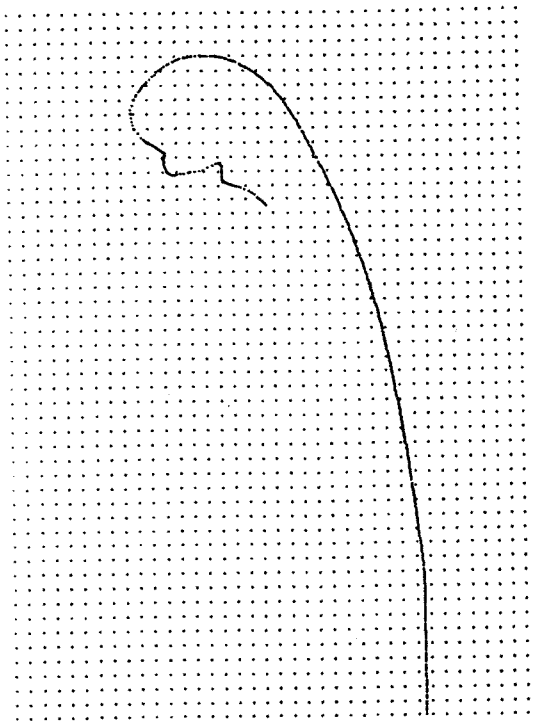

Figure 3d. t=.8

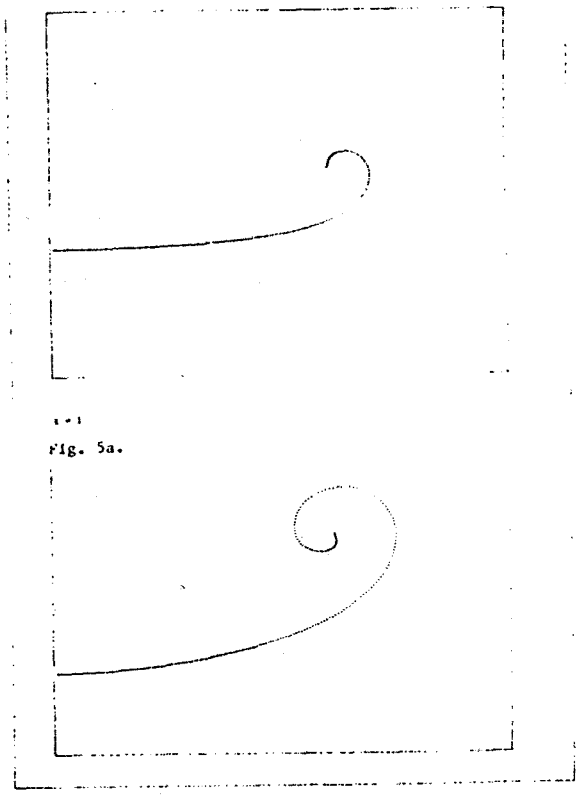

t = 1

Fig. 5a.

t = 2

Fig. 5b.

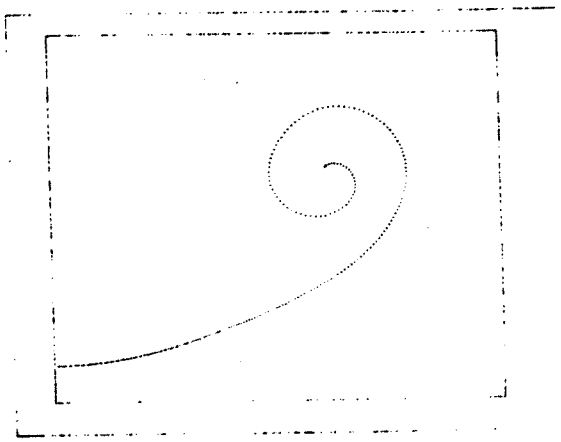

Fig. 5c.

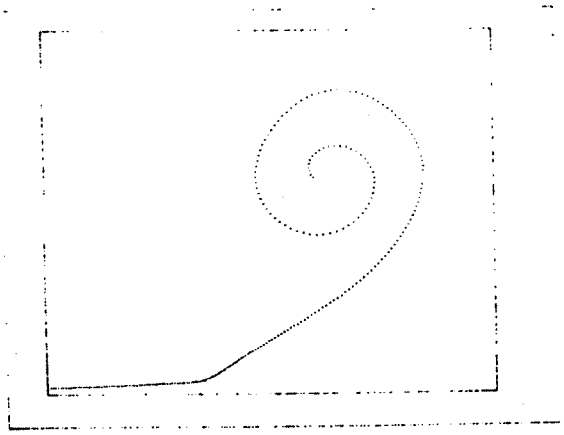

Fig. 5d.

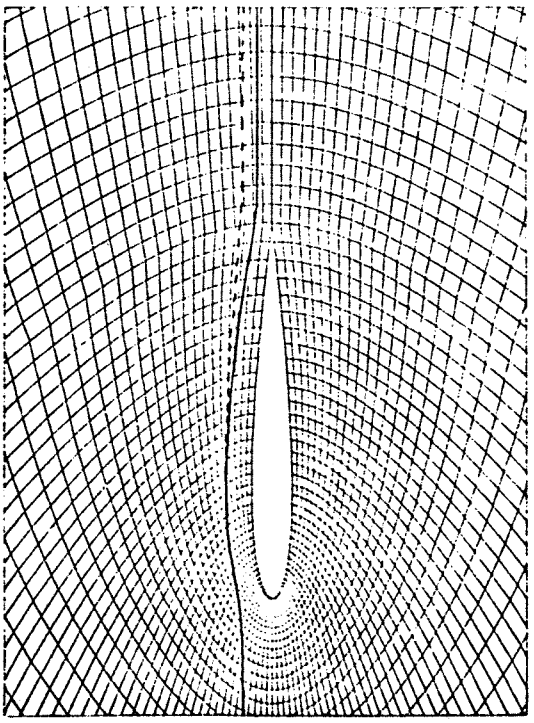

Figure 6a Vortex and Streamline Trajectories

Vortex (——)

Streamline (- - -) (without vortex)

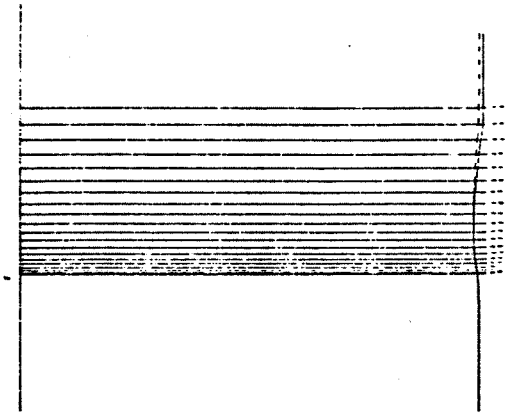

Figure 6b Vortex and Streamline Trajectories

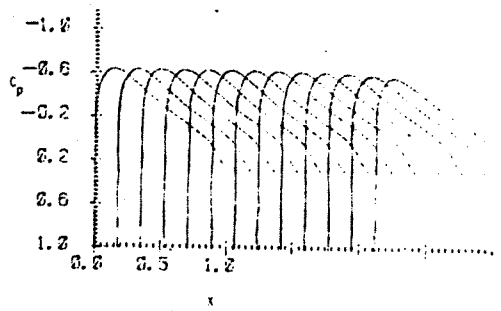

Figure 7a - C_p - No Vortex

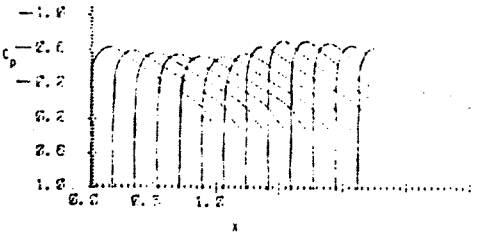

Figure 7b - C_p - Lower Surface - with Vortex

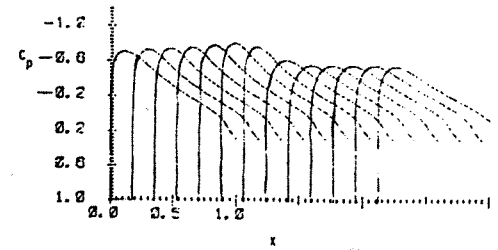

Figure 7c - C_p - Upper Surface - with Vortex